Lattice distortions and stripes in the underdoped region of high-T_c cuprates

2003 J. Phys. A: Math. Gen. 36 9337

(http://iopscience.iop.org/0305-4470/36/35/318)

INSTITUTE OF PHYSICS PUBLISHING JOURNAL OF PHYSICS A: MATHEMATICAL AND GENERAL

J. Phys. A: Math. Gen. **36** (2003) 9337–9349 PII: S0305-4470(03)59135-1

Lattice distortions and stripes in the underdoped region of high-T_c cuprates

Takashi Yanagisawa

Condensed Matter Physics Group, Nanoelectronics Research Institute, National Institute of Advanced Industrial Science and Technology, Central 2, 1-1-1 Umezono, Tsukuba, Ibaraki 305-8568, Japan

E-mail: t-yanagisawa@aist.go.jp

Received 31 January 2003, in final form 1 April 2003
Published 20 August 2003
Online at stacks.iop.org/JPhysA/36/9337

Abstract

Superconducting and striped states under lattice distortions are investigated for high-T_c cuprates based on the quantum variational Monte Carlo method as the ground state of the two-dimensional (three-band) Hubbard model. We study the wavefunctions for the correlated condensed states: superconductivity, antiferromagnetism, inhomogeneity and their coexistent state with on-site Gutzwiller correlation. The model parameters are chosen for cuprate high-T_c superconductors such as $La_{1-x}Sr_xCuO_4$ with $x < 0.125$. The ground state has vertical or horizontal hole-rich arrays coexisting with incommensurate magnetism and superconductivity (SC) in the low-temperature tetragonal (LTT) phase. We show that the total energy of the inhomogeneous d-wave SC state with vertical stripes having half-filled holes is lower than that of competing spin-density wave (SDW) states. The SC order parameter oscillates according to inhomogeneity in the antiferromagnetic background, and the SC condensation energy is reduced as the doping rate decreases in the underdoped region. The decreasing tendency of the SC condensation energy with decreasing doping is in accord with that of the specific heat data. In the low-temperature orthogonal (LTO) phase the diagonal stripes are stabilized in the lightly doped region for less than 5% doping. We also examine the stability of the mixed phase of LTT–HTT coexisting with stripes.

PACS numbers: 78.20.−e, 78.30.−j, 74.76.Bz

1. Introduction

The electronic properties of oxide high-T_c superconductors have been extensively investigated over the last decade. The mechanism of superconductivity (SC) has been extensively studied using various two-dimensional (2D) models of electronic interactions. The 2D three-band

Hubbard model is the simplest and most fundamental model among such models. The 2D single-band Hubbard model is regarded as the simplified one of the three-band model. Studies of these models over the last decade indicated that the d-wave SC may be induced from the electronic repulsive interaction [4, 22, 23, 34, 37, 39, 40, 49]; significantly it has been shown that the SC condensation energy and the magnitude of the order parameter are in reasonable agreement with the experimental results in the optimally doped case [50, 53, 54].

The interplay between magnetism and superconductivity is suggested in the underdoped region. The reduction of T_c in this region remains unresolved and may be related to magnetism. The existence of incommensurate correlations with modulation vectors given by $Q_s = (\pi \pm 2\pi\delta, \pi)$ and $Q_c = (\pm 4\pi\delta, 0)$ (or $Q_s = (\pi, \pi \pm 2\pi\delta)$ and $Q_c = (0, \pm 4\pi\delta)$) was reported by neutron-scattering measurements for the hole-doping rate δ [2, 29, 36, 44–47]. The linear doping dependence of incommensurability in the underdoped region supports a striped structure and suggests a relationship between magnetism and SC [47]. A relationship between the SDW, charge-density wave (CDW) orders and crystal structure is also suggested in intensive studies by the neutron-scattering measurements [17, 19, 24, 44]; in particular in the low-temperature tetragonal (LTT) and low-temperature less-orthorhombic (LTLO) phases, the CDW order is stabilized [10], while no well-defined incommensurate CDW peaks were observed for the orthorhombic systems [19, 24]. In the elastic and inelastic neutron scattering experiments with $La_{2-x}Sr_xCuO_4$, the incommensurate magnetic scattering spots around (π, π) have been observed in the SC phase in the range $0.05 < x < 0.13$ [11, 19, 47].

2. Hamiltonian and correlated condensed states

The Hamiltonian for the CuO_2 planes contained in oxide superconductors is given by the three-band Hubbard model,

$$\begin{aligned} H_{dp} = {} & \epsilon_d \sum_{i\sigma} d^\dagger_{i\sigma} d_{i\sigma} + U_d \sum_i d^\dagger_{i\uparrow} d_{i\uparrow} d^\dagger_{i\downarrow} d_{i\downarrow} + \epsilon_p \sum_{i\sigma} \left(p^\dagger_{i+\hat{x}/2,\sigma} p_{i+\hat{x}/2,\sigma} + p^\dagger_{i+\hat{y}/2,\sigma} p_{i+\hat{y}/2,\sigma} \right) \\ & - t_{pd} \sum_{i\sigma} \left[d^\dagger_{i\sigma} (p_{i+\hat{x}/2,\sigma} + p_{i+\hat{y}/2,\sigma} - p_{i-\hat{x}/2,\sigma} - p_{i-\hat{y}/2,\sigma}) + \text{h.c.} \right] \\ & - t_{pp} \sum_{i\sigma} \left[p^\dagger_{i+\hat{y}/2,\sigma} p_{i+\hat{x}/2,\sigma} - p^\dagger_{i+\hat{y}/2,\sigma} p_{i-\hat{x}/2,\sigma} \right. \\ & \left. - p^\dagger_{i-\hat{y}/2,\sigma} p_{i+\hat{x}/2,\sigma} + p^\dagger_{i-\hat{y}/2,\sigma} p_{i-\hat{x}/2,\sigma} + \text{h.c.} \right]. \end{aligned} \tag{1}$$

$\hat{x}$ and $\hat{y}$ represent unit vectors along the x and y directions, respectively. $p^\dagger_{i\pm\hat{x}/2,\sigma}$ and $p_{i\pm\hat{x}/2,\sigma}$ denote the operators for the p electrons at site $R_i \pm \hat{x}/2$. Similarly $p^\dagger_{i\pm\hat{y}/2,\sigma}$ and $p_{i\pm\hat{y}/2,\sigma}$ are defined. U_d denotes the strength of the Coulomb interaction between d electrons. For simplicity we neglect the Coulomb interaction among p electrons. Other notation is standard and energies are measured in t_{pd} units. The number of cells is denoted as N for the three-band Hubbard model. The number of atoms is denoted as N_a. In the non-interacting case ($U_d = 0$) the Hamiltonian in the $\mathbf{k}$-space is written as

$$\begin{aligned} H^0_{dp} = {} & \epsilon_d \sum_{\mathbf{k}\sigma} d^\dagger_{\mathbf{k}\sigma} d_{\mathbf{k}\sigma} + \epsilon_p \sum_{\mathbf{k}\sigma} \left(p^\dagger_{x\mathbf{k}\sigma} p_{x\mathbf{k}\sigma} + p^\dagger_{y\mathbf{k}\sigma} p_{y\mathbf{k}\sigma} \right) \\ & + \sum_{\mathbf{k}\sigma} \left(2it_{pd} \sin(k_x/2)\, d^\dagger_{\mathbf{k}\sigma} p_{x\mathbf{k}\sigma} + \text{h.c.} \right) + \sum_{\mathbf{k}\sigma} \left(2it_{pd} \sin(k_y/2)\, d^\dagger_{\mathbf{k}\sigma} p_{y\mathbf{k}\sigma} + \text{h.c.} \right) \\ & + \sum_{\mathbf{k}\sigma} (-4t_{pp} \sin(k_x/2) \sin(k_y/2)) \left(p^\dagger_{x\mathbf{k}\sigma} p_{y\mathbf{k}\sigma} + \text{h.c.} \right) \end{aligned} \tag{2}$$

Table 1. Typical parameter values for the three-band Hubbard model. Energies are measured in eV.

	Hybertson *et al* [15]	Eskes *et al* [7]	McMohan *et al* [31]	Tjeng *et al* [43] (Cu_2O)
$\epsilon_p - \epsilon_d$	3.6	2.75–3.75	3.5	2.5
t_{pd}	1.3	1.5	1.5	1.47
t_{pp}	0.65	0.65	0.6	
U_d	10.5	8.8	9.4	9.7
U_p	4.0	6.0	4.7	5.7
U_{dp}	1.2	<1.0	0.8	<1

where $d_{\mathbf{k}\sigma}\left(d^{\dagger}_{\mathbf{k}\sigma}\right)$, $p_{x\mathbf{k}\sigma}\left(p^{\dagger}_{x\mathbf{k}\sigma}\right)$ and $p_{y\mathbf{k}\sigma}\left(p^{\dagger}_{y\mathbf{k}\sigma}\right)$ are operators for the d-, p_x- and p_y-electrons of momentum $\mathbf{k}$ and spin σ, respectively.

The parameters of the three-band Hubbard model are given by the Coulomb repulsion U_d, energy levels of p electrons ϵ_p and d electron ϵ_d, and transfer between p orbitals given by t_{pp}. Typical parameter values for the three-band (d–p) Hubbard model are shown in table 1. In the limit $t_{pd} \ll U_d - (\epsilon_p - \epsilon_d)$, $t_{pd} \ll \epsilon_p - \epsilon_d$ and $\epsilon_p - \epsilon_d < U_d$, the d–p model is mapped to the t–J model with [59]

$$J = 4t_{\mathrm{eff}}^2 \left(\frac{1}{U_d} + \frac{2}{2(\epsilon_p - \epsilon_d) + U_p} \right) \tag{3}$$

where $t_{\mathrm{eff}} \simeq t_{pd}^2 / (\epsilon_p - \epsilon_d)$. $J_K = 4t_{\mathrm{eff}}$ gives the antiferromagnetic coupling between the neighbouring d and p electrons. Since $(\epsilon_p - \epsilon_d)/t_{pd}$ is not so large in real materials, the mapping to the t–J model is not necessarily justified.

The simplified single-band Hubbard model has also been studied intensively with focus on the d-electrons

$$H = -\sum_{ij\sigma} t_{ij} d^{\dagger}_{i\sigma} d_{j\sigma} + U \sum_{i} n_{di\uparrow} n_{di\downarrow} \tag{4}$$

where $n_{di\sigma} = d^{\dagger}_{i\sigma} d_{i\sigma}$ is the number operator.

In the following, let us consider mainly the three-band model. Our wavefunction is a Gutzwiller-projected function defined as

$$\psi = P_G \psi_0 \tag{5}$$

where ψ_0 is the one-body wavefunction and P_G is the Gutzwiller projection operator given by

$$P_G = \prod_j [1 - (1 - g) n_{dj\uparrow} n_{dj\downarrow}]. \tag{6}$$

g is a variational parameter in the range from 0 to unity and j labels a site in the real space. For the normal state trial function we take ψ_0 as the Fermi sea. In constructing variational wavefunctions with inhomogeneity or without translational invariance, the plane waves are replaced by solutions of the eigen-equation given by

$$\sum_j H^0_{ij\sigma} x^{\lambda}_{j\sigma} = E^{\lambda} x^{\lambda}_{i\sigma} \tag{7}$$

where $H^0_{ij\sigma}$ is a trial Hamiltonian matrix for spin σ in real space. In evaluating the expectation values based on Monte Carlo procedures, we can use both the algorithm developed by Ceperley *et al* [6] and that employed in the auxiliary field quantum Monte Carlo method [5, 51, 52]

in actual calculations. When we employ the auxiliary field method, we update the weight function $w = w_\uparrow w_\downarrow$ in the Monte Carlo process [51] where

$$w_\sigma = \det(\varphi_\sigma \exp(V_\sigma(u,\alpha)) \exp(V_\sigma(s,\alpha))\varphi_\sigma) \tag{8}$$

where φ_σ is defined as $(\varphi_\sigma)_{j\lambda} = x^\lambda_{\sigma j}(j = 1, \ldots, N_a, \lambda = 1, \ldots, N_e/2)$; $V_\sigma(s,\alpha)$ is a diagonal matrix $V_\sigma(s,\alpha) = \mathrm{diag}(2a\sigma s_1 - \alpha/2, \ldots, 2a\sigma s_N - \alpha/2, \ldots)$ corresponding to the potential

$$h_\sigma(s) = 2a\sigma \sum_i s_i n_{di\sigma} - \frac{\alpha}{2} \sum_i n_{di\sigma} \tag{9}$$

for the constants $\alpha = \log(1/g)$ and $a = \frac{1}{2}\cosh^{-1}(\mathrm{e}^{\alpha/2})$. The Hubbard–Stratonovich auxiliary fields s_i are employed to write the Gutzwiller operator in the bilinear form,

$$\exp\left(-\alpha \sum_i n_{di\uparrow} n_{di\downarrow}\right) = \left(\frac{1}{2}\right)^N \sum_{s_i=\pm 1} \exp\left[2a \sum_i s_i (n_{di\uparrow} - n_{di\downarrow}) - \frac{\alpha}{2} \sum_i (n_{di\uparrow} + n_{di\downarrow})\right]. \tag{10}$$

A superconducting state is expressed by the BCS wavefunction given as

$$\psi_{\mathrm{BCS}} = P_{N_e} \prod_k \left(u_k + v_k \beta^\dagger_{k\uparrow} \beta^\dagger_{-k\downarrow}\right)|0\rangle \tag{11}$$

where $\beta^\dagger_{k\sigma}$ is the creation operator for the mixed band obtained from the diagonalization of the non-interacting Hamiltonian H^0_{dp}. $\beta^\dagger_{k\sigma}$ denotes the operator for the highest band in the electron representation or that for the lowest band in the hole picture. P_{N_e} is a projection operator which extracts only the states with a fixed total electron (or hole) number N_e. Coefficients u_k and v_k appearing only in the ratio are defined by

$$\frac{v_k}{u_k} = \frac{\Delta_k}{\xi_k + \sqrt{\xi_k^2 + \Delta_k^2}} \tag{12}$$

$$\xi_k = \epsilon_k - \mu. \tag{13}$$

Δ_k is a k-dependent gap function. ϵ_k is the band dispersion and μ is a variational parameter working like the chemical potential in the trial wavefunction.

In order to investigate the inhomogeneous wavefunction, we extend the uniform BCS wavefunction to a non-uniform one. The wavefunction is constructed from the solution of the Bogoliubov–de Gennes equation given by

$$\sum_j \left(H^0_{ij\uparrow} u^\lambda_j + F_{ij} v^\lambda_j\right) = E^\lambda u^\lambda_i \tag{14}$$

$$\sum_j \left(F^*_{ji} u^\lambda_j - H^0_{ji\downarrow} v^\lambda_j\right) = E^\lambda v^\lambda_i \tag{15}$$

where $(H_{ij\sigma})$ and (F_{ij}) are $3N \times 3N$ matrices including the terms for d, p_x and p_y orbitals. The Bogoliubov operators are written in the form

$$\alpha_\lambda = \sum_i \left(u^\lambda_i a_{i\uparrow} + v^\lambda_i a^\dagger_{i\downarrow}\right) \qquad (E^\lambda > 0) \tag{16}$$

$$\alpha_{\bar{\lambda}} = \sum_i \left(u^{\bar{\lambda}}_i a_{i\uparrow} + v^{\bar{\lambda}}_i a^\dagger_{i\downarrow}\right) \qquad (E^{\bar{\lambda}} < 0). \tag{17}$$

$a_{i\sigma}$ denotes $d_{i\sigma}$, $p_{i+\hat{x}/2\sigma}$ or $p_{i+\hat{y}/2\sigma}$ corresponding to the components of u^λ_i and v^λ_i. For the single-band Hubbard model, $a_{i\sigma}$ is simply the operator for conduction electrons.

Then the wavefunction is written as [14, 33, 56]

$$\psi = P_G P_{N_e} \prod_{\lambda} \alpha_\lambda \alpha_{\bar{\lambda}}^\dagger |0\rangle = \text{Const}\, P_G P_{N_e} \exp\left(- \sum_{ij} (U^{-1}V)_{ij} a_{i\uparrow}^\dagger a_{j\downarrow}^\dagger \right) |0\rangle$$
$$\propto P_G \left[\sum_{ij} (U^{-1}V)_{ij} a_{i\uparrow}^\dagger a_{j\downarrow}^\dagger \right]^{N_e/2} |0\rangle. \tag{18}$$

U and V are matrices defined by $(V)_{\lambda j} = v_j^\lambda$ and $(U)_{\lambda j} = u_j^\lambda$. P_G is the Gutzwiller operator. The spin modulation potential is contained in $(H_{ij\sigma})$ and the SC order parameters Δ_{ij} are included in (F_{ij}). The second equality in equation (18) is derived as follows. We assume that the SC state is written in the form

$$\psi = A \exp\left(\sum_{ij} \phi_{ij} a_{i\uparrow}^\dagger a_{j\downarrow}^\dagger \right) |0\rangle \tag{19}$$

for a constant A. Since the SC state satisfies $\alpha_\lambda \psi = 0$, we have

$$\sum_i \left(u_i^\lambda a_{i\uparrow} + v_i^\lambda a_{i\downarrow}^\dagger \right) \psi = 0. \tag{20}$$

Operating U^{-1} to this equation, ψ satisfies

$$\left[a_{j\uparrow} + \sum_i \sum_\lambda (U^{-1})_{j\lambda} V_{\lambda i} a_{i\downarrow}^\dagger \right] \psi = 0. \tag{21}$$

Instead, from equation (19) we can derive

$$\left(a_{j\uparrow} - \sum_i \phi_{ji} a_{i\downarrow}^\dagger \right) \psi = 0 \tag{22}$$

using the anticommutation relation $\left\{ a_{i\sigma}, a_{j\sigma'}^\dagger \right\} = \delta_{ij}\delta_{\sigma,\sigma'}$. Then from equations (21) and (22) ϕ_{ij} is given by

$$\phi_{ij} = - \sum_\lambda (U^{-1})_{i\lambda} V_{\lambda j} = -(U^{-1}V)_{ij}. \tag{23}$$

The Monte Carlo algorithm by Ceperley *et al* [6] is applicable to the wavefunction in equation (18). The auxiliary field Monte Carlo method is also achieved for the inhomogeneous SC state introducing the simple electron–hole transformation for the down spin by defining [58]

$$a_{-k\downarrow}^\dagger = c_k. \tag{24}$$

The operators for up-spin electrons remain the same $a_{-k\uparrow}^\dagger \equiv a_k^\dagger$. Now the pair potential term F_{ij} is written as the mixing term between c and a electrons. Diagonalizing the matrix H_{ij}^0, the wavefunction $\psi \sim P_G \varphi$ is represented by the Slater determinant. Then the Monte Carlo method can be applied using the formula in equation (8) [52].

The quasi-one-dimensional structures were predicted by mean-field theories [27, 28, 41, 42, 60]; these states are called stripes. The wavefunction with the stripe structure is made from solutions of the Hartree–Fock Hamiltonian given as

$$H_{\text{trial}} = H_{dp}^0 + \sum_{i\sigma} [\delta n_{di} - \sigma (-1)^{x_i + y_i} m_i] d_{i\sigma}^\dagger d_{i\sigma} \tag{25}$$

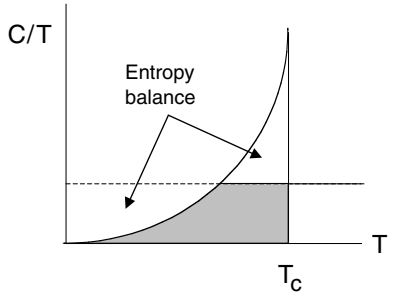

Figure 1. Due to the entropy balance the two parts indicated by arrows have the same area.

where we have variational parameters $\tilde{\epsilon_p}$ and $\tilde{\epsilon_d}$ in H^0_{pd}. In this paper δn_{di} and m_i are assumed to have the form [12, 30, 55]: $\delta n_{di} = -\sum_j \alpha/\cosh\left(\left(x_i - x_j^{\rm str}\right)\right)$ and $m_i = \Delta_{\rm inc}\prod_j \tanh\left(\left(x_i - x_j^{\rm str}\right)\right)$ with parameters α and $\Delta_{\rm inc}$, where $x_j^{\rm str}$ denote the position of a stripe. The copper-centre striped states are investigated in this paper. The inclusion of stripe order parameters considerably improves the ground state energy. In small clusters, the deviation of the energy of the striped state from the exact value is within several per cent for the Hubbard model [57]. The SC gap parameters Δ_{ij} are included in (F_{ij}). We assume the following spatial variation for the SC order parameters in the d-electron part: $\Delta_{i,i+\hat{x}} = \Delta_s\cos(Q_x(x_i + \hat{x}/2))$, $\Delta_{i,i+\hat{y}} = -\Delta_s\cos(Q_x x_i)$, where $Q_x = 2\pi\delta$ (δ is the hole density). The SC order parameter oscillates according to the spin and charge distributions so that the amplitude has a maximum in the hole-rich region and is suppressed in the hole-poor region.

3. Superconducting condensation energy

The superconducting condensation energy is given by the difference of free energy between the normal and SC states:

$$\Delta E_{\rm SC} = \Omega_n - \Omega_s = \int_0^{T_c} (S_n - S_s)\,{\rm d}T \tag{26}$$

for the constant volume ${\rm d}V = 0$. The entropy difference $\Delta S(T) \equiv S_n - S_s$ is written as

$$\Delta S(T) = \int_0^T \frac{{\rm d}(\Delta Q)}{T} \tag{27}$$

for the heat transfer ${\rm d}(\Delta Q)$. If we assume that ${\rm d}(\Delta Q) = (C_n - C_s)\,{\rm d}T$, using the partial integration, the SC condensation energy is estimated from the relation given as

$$\Delta E_{\rm SC} = \int_0^{T_c} (C_s - C_n)\,{\rm d}T \tag{28}$$

where we use the entropy balance relation at T_c: $S_n(T_c) = S_s(T_c)$ (figure 1). From the specific heat reported by Loram *et al* [25], the condensation energy was obtained as 0.17–0.26 meV/(Cu site) by numerically integrating the SC specific heat minus the normal state one with respect to temperature from zero to T_c [1, 49].

In the limit $U_d \to 0$, $\Delta E_{\rm SC}$ is extremely small showing an exponential dependence on U_d since Δ_s is given as [22, 23]

$$\Delta_s \propto \exp\left(-2/\left(xU_d^2\right)\right) \tag{29}$$

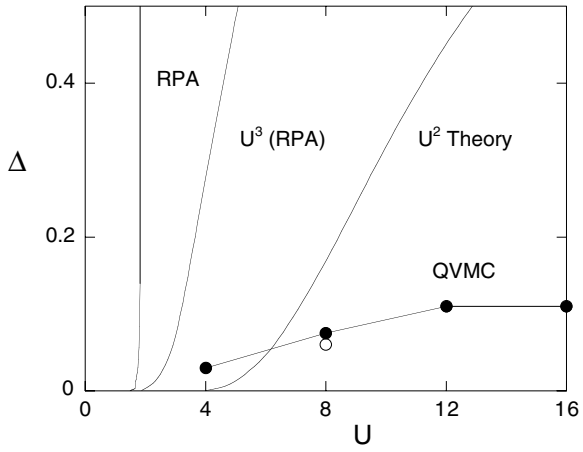

Figure 2. Δ as a function of U for the single-band Hubbard model. The energy unit is the nearest neighbour transfer integral t. The curve by U^2 theory indicates the results obtained from the lowest order perturbation theory. $U^3(RPA)$ means that we consider the terms up to the third order of U without vertex terms. Solid circles indicate the results obtained by the variational Monte Carlo method [37, 49] based on the Gutzwiller function. Open circle is estimated by the improved wavefunction with the off-diagonal Jastrow correlation factor [51, 52].

for a constant x. The U-dependence of the SC gap Δ_s for the single-band Hubbard model is shown in figure 2. Δ_s shows the exponential behaviour for small U changing into a constant for the intermediate U. For large U it may show $1/U$ dependence: $\Delta_s \sim 1/U$ as expected from a mapping to the t–J model with $J \propto 1/U$. It is suggested from figure 2 that the SC evolves from small U continuously to the intermediate region of U.

For the intermediate Coulomb interaction U_d, the more reliable numerical method, VMC, is used in this paper. It is not an easy task to estimate the SC condensation energy in the large systems. In the study of the ladder model [20, 38, 48], the bulk limit was first evaluated by VMC [21]. The ground state energy

$$E_g = \langle H \rangle = \langle \psi | H | \psi \rangle / \langle \psi | \psi \rangle \tag{30}$$

is obtained using the Monte Carlo procedure. We optimized E_g with respect to variational parameters. The energy gain due to the SC gap formation, i.e. the SC condensation energy, was estimated from the difference between the minimum $E_g(\Delta_{s,\mathrm{opt}})$ with Δ_s optimized and the normal state value $E_g(\Delta_s = 0)$:

$$\Delta E_{\mathrm{SC}} = E_g(\Delta_s = 0) - E_g(\Delta_{s,\mathrm{opt}}). \tag{31}$$

In figure 3, the size dependence of the SC condensation energy is shown for the uniform SC in the overdoped region and the striped SC in the underdoped region with the results obtained for the 2D one-band Hubbard model for comparison. The parameters are $t_{pp} = 0.4$ and $U_d = 8$ in t_{pd} units. The squares in figure 3 indicate the SC condensation energy of the pure d-wave state at $\delta \approx 0.2$, while the circles are for SC coexisting with stripes at $\delta = 1/8$ for $Q_x = \pi/4$ evaluated on rectangular lattices 32×8, 24×6, 16×8 and 16×4. In both cases the energy obtained through an extrapolation is of the same order as the experimental values.

$$\Delta E_{\mathrm{SC}} \approx 0.00014 t_{pd} \approx 0.2\,\mathrm{meV} \tag{32}$$

where we assigned $t_{pd} \approx 1.5\,\mathrm{eV}$ suggested from cluster calculations [7, 31]. In figure 4 we show the SC condensation energy as a function of the hole density. Solid circles indicate the

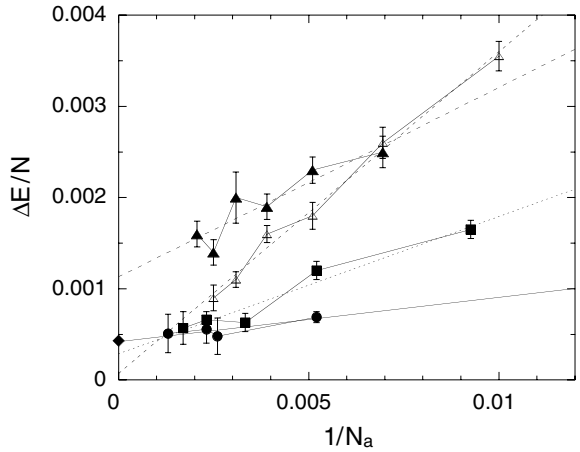

Figure 3. SC condensation energy per site as a function of $1/N_a$ in t units where $t \approx t_{pd}/3$ and N_a is the number of atoms. Squares are for $\delta \approx 0.2$, $t_{pp}/t_{pd} = 0.4$ and $U_d/t_{pd} = 8$ for the three-band model on square lattices. Circles are at $\delta = 1/8$ coexisting with stripes for $t_{pp}/t_{pd} = 0.4$ and $U_d/t_{pd} = 8$ on rectangular lattices 32×8, 24×6, 16×8 and 16×4. Triangles are for the single-band Hubbard model; $\delta = 0.86$ and $t' = -0.2$ and $U = 8$ for solid symbols and $\delta = 0.84$ and $t' = -0.15$ for open symbols (where energy unit is t and t' is the next nearest neighbour transfer) [50]. The diamond shows the value indicated from experiments.

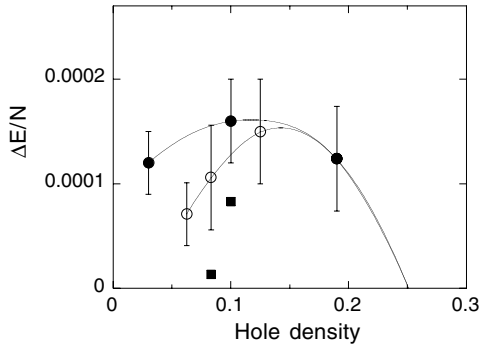

Figure 4. SC condensation energy per site versus the hole density in t_{pd} units, where the parameters are $t_{pp} = 0.4$ and $U_d = 8$. Solid circles and open circles indicate the SC condensation energy for the uniform SC and striped SC, respectively. The lines are fitted by parabolas. Squares are obtained for the single-band Hubbard model with the next nearest transfer $t'/t = -0.2$ on a 12×12 lattice [33].

results for the Gutzwiller function without long-range order and open circles show the results for the striped Gutzwiller function, respectively. The SC condensation energy per site for the striped SC is reduced as the hole density decreases, while that for pure d-wave SC remains finite even near half-filling. Since the striped SC has lower energy than the d-wave SC in the underdoped region, the SC condensation energy decreases as the hole density decreases in the ground state. The decreasing tendency of the SC condensation energy was reported from the specific heat measurements [26, 35]. This suggests that an origin of the decrease of T_c in the underdoped region simply lies in the reduction of hole-rich domain, where the SC order parameter has finite amplitude. In our evaluations the half-filled striped state is stable around $1/8$-hole doping.

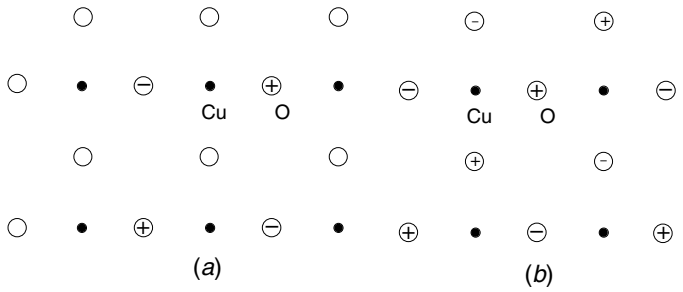

Figure 5. Lattice structures in the LTT phase (*a*) and LTO phase (*b*). The symbol '+' means that the oxygen atoms move up and '−' means that the oxygen atoms move down. Large '+' and '−' indicate large displacements. 'O' denotes the oxygen atom.

4. Stripes and lattice distortions

Now let us turn to consider the effect of lattice distortion on stripes. In the LTT phase stabilized at low temperatures near 1/8-hole filling, the distortions of the CuO square occur in the manner shown in figure 5 where the '+' oxygen moves up, the '−' oxygen moves down and the oxygen left blank remain in the same position. The LTT phase has a 'tilting axis' on which the copper and oxygen atoms never move even in the distorted state [3]. In figure 5(*a*) there is the vertical tilting axis. The vertical or horizontal stripes can coexist with the lattice distortions in the LTT phase.

Let us investigate the lattice distortions in the following Hamiltonian

$$\begin{aligned} H^0_{pd} = {} & \epsilon_d \sum_{i\sigma} d^\dagger_{i\sigma} d_{i\sigma} + \epsilon_p \sum_{i\sigma} \left(p^\dagger_{i+\hat{x}/2,\sigma} p_{i+\hat{x}/2,\sigma} + p^\dagger_{i+\hat{y}/2,\sigma} p_{i+\hat{y}/2,\sigma} \right) \\ & + t_{pd} \sum_{i\sigma} \left[d^\dagger_{i\sigma} \left(p_{i+\hat{x}/2,\sigma} + p_{i+\hat{y}/2,\sigma} - p_{i-\hat{x}/2,\sigma} - p_{i-\hat{y}/2,\sigma} \right) + \text{h.c.} \right] \\ & + t_{pp} \sum_{i\sigma} (1 + v_i) \left[p^\dagger_{i+\hat{y}/2,\sigma} p_{i+\hat{x}/2,\sigma} - p^\dagger_{i+\hat{y}/2,\sigma} p_{i-\hat{x}/2,\sigma} - p^\dagger_{i-\hat{y}/2,\sigma} p_{i+\hat{x}/2,\sigma} \right. \\ & \left. + p^\dagger_{i-\hat{y}/2,\sigma} p_{i-\hat{x}/2,\sigma} + \text{h.c.} \right] + t_{pd} \sum_{i\sigma} \left[u_{i\hat{x}} d^\dagger_{i\sigma} p_{i+\hat{x}/2,\sigma} - u_{i,-\hat{x}} d^\dagger_{i\sigma} p_{i-\hat{x}/2,\sigma} \right. \\ & \left. + u_{i\hat{y}} d^\dagger_{i\sigma} p_{i+\hat{y}/2,\sigma} - u_{i,-\hat{y}} d^\dagger_{i\sigma} p_{i-\hat{y}/2,\sigma} + \text{h.c.} \right] \end{aligned} \tag{33}$$

where $u_{i\hat{\mu}}$ and v_i represent the variations of the transfer energy t_{pd} and t_{pp}, respectively. We examine a transition from the LTO to the LTT phase; the case $u_{i\hat{\mu}} = 0$ and $v_i = 0$ corresponds to the LTO phase. We neglect the anisotropy of t_{pp} in the LTO phase for simplicity. The LTT structure is realized by rotation around the fixed axis parallel to the x- or y-axis from the LTO lattice, while the HTT structure occurs through rotation around the diagonal axis from LTO. Here HTT means the normal lattice without distortions called high-temperature tetragonal (HTT) structure. We simply assume the same elastic energy cost for these two types of rotations.

The structural transition from low-temperature orthorhombic (LTO) to LTT phases has been reported in LaBaSrCuO and LaNdSrCuO systems [17]. We consider the following cases assuming that the stripes are in the y-direction:

(A) $u_{i\hat{x}} = u, u_{i\hat{y}} = 0, v_i = 0,$
(B) $u_{i\hat{x}} = 0, u_{i\hat{y}} = u, v_i = 0,$
(C) $u_{i\hat{x}} = u, u_{i\hat{y}} = u\cos(2Q_x x_i), v_i = u\cos(2Q_x x_i),$

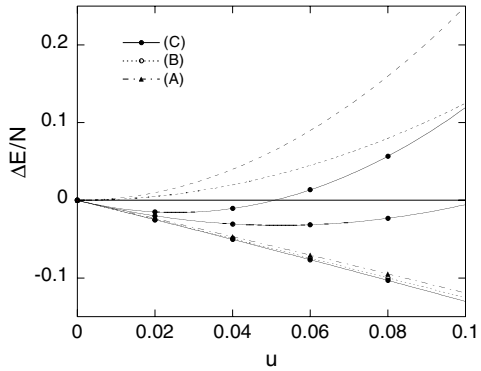

Figure 6. Energy gain $\Delta E = E(u = 0) - E(u)$ ($u = \delta t_{pd}/t_{pd}$) per site as a function of transfer deformation u in t_{pd} units. The parameters are $t_{pp} = 0.4$ and $U_d = 8$ for a 16×4 lattice. The hole-rich stripes are in the y-direction. The energy gains for (A) $u_{i\hat{y}} = 0$ (triangles), (B) $u_{i\hat{x}} = 0$, (open circles) and (C) (solid circles) are shown. The elastic energy $Ku^2/2$ is shown by the dashed line (for $K = 5$ and $K = 10$). The summations of $\Delta E = E(u = 0) - E(u)$ and the elastic energy per site are also shown for the case (C). The Monte Carlo statistical errors are smaller than the size of the symbols.

where $Q_x = 2\pi\delta$, u is the amplitude of deformation of t_{pd} and t_{pp}, and $u_{i\hat{\mu}} = u_{i,-\hat{\mu}}$ are assumed. $u = 0$ corresponds to the LTO structure, and the anisotropy in t_{pd} indicates a transition to the LTT phase. t_{pd} increases along the tilt axis compared to the LTO phase. The stripes are perpendicular to the tilting axis in the case (A) and parallel in the case (B). The case (C) corresponds to the structure of the mixed LTT–HTT phase. The energy gain per site defined as $\Delta E/N = (E(u = 0) - E(u))/N$ is presented in figure 6 as a function of u in t_{pd} units. As shown in the figure, the energy in case (B) is lower than that in case (A) indicating that the stripes are parallel to the tilting axis under the rigid LTT structure [18]. This is simply because the kinetic energy gain in the parallel striped state in case (B) dominates over that in the perpendicular striped state in case (A). The cost of energy due to lattice distortions is assumed to be given by $(K/2)u^2$ for the constant K, which is estimated in the following way. According to Harrison's rule [13], t_{pd} is expected to vary as d^{-n} with $n \approx 7/2$, d being the Cu–O bond length. Since $\delta t_{pd}/t_{pd} = -n\delta d/d$, the elastic energy is estimated as

$$E_{el} = \frac{1}{2}C(2d)^3\left(\frac{\delta d}{d}\right)^2 = \frac{1}{2}C(2d)^3\frac{1}{n^2}u^2 \equiv \frac{K}{2}u^2. \tag{34}$$

The constant C is estimated as $C \approx 1.7 \times 10^{12}\,\mathrm{dyn/cm^2} = 1.7\,\mathrm{eV\,\AA^{-3}}$ [32]. Since $d \approx 2$ Å, K is of the order of 10 eV: $K \approx 8.9$ eV. The energy is lowered further in case (C) where the softening of the tilt angle is taken into account. We show schematically the stable striped state in the LTT phase in figure 7 obtained from our VMC evaluations, where the shaded square represents the tilted CuO unit cell rotating around the tilting axis. The tilt angle is reduced in the hole-rich region called HTT in this paper. The LTT–HTT state is more stabilized due to the kinetic energy gain coming from the softening of tilt angles.

Let us discuss the other type of stripes called diagonal stripes where there are hole arrays in the diagonal direction. In VMC calculations, the vertical striped state always has slightly lower energy than the diagonal stripe state on the lattice without distortions in contrast to the mean field results [16]. The diagonal stripes were shown to be stable at low doping within the dynamical mean field theory, giving a cross over from diagonal stripes in the low doping regime to the vertical stripes at doping higher than 0.05 [8, 9]. Here we propose a scenario that

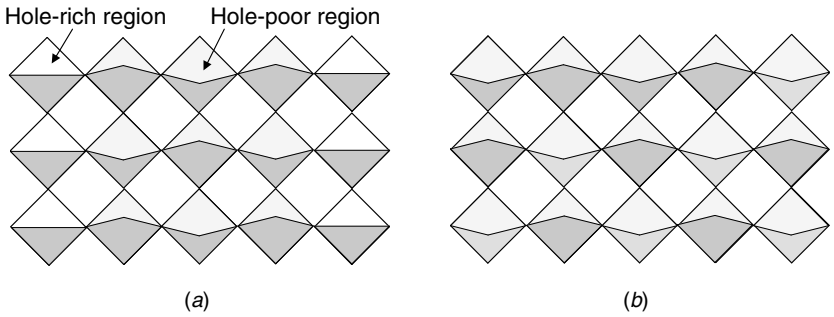

Figure 7. Schematic structure of lattice distortions and stripes where the hole-rich arrays are perpendicular to the tilting axis in (*a*) and parallel to that in (*b*). We call the state in (*a*) the LTT–HTT mixed phase. The shaded square represents a distorted CuO unit cell. In the hole-rich HTT region the tilt angle is reduced.

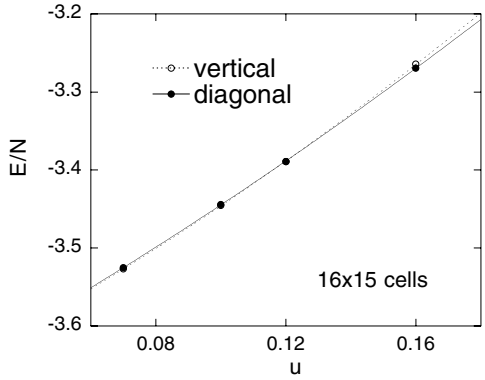

Figure 8. Energy as a function of transfer deformation u for the diagonal and vertical stripes in the LTO phase. The doping rate is 0.033%, and the parameters are given by $t_{pp} = 0.4$, $U_d = 8$ and $\epsilon_p - \epsilon_d = 2$ in t_{pd} units. The lattice size is 16×15.

the anisotropy of transfer energy t_{pp} in the LTO phase will stabilize the diagonal stripes. In the LTO structure the transfer t_{pd} is reduced as $t_{pd}(1-u)$, t_{pp} in one direction is also reduced as $t_{pp}(1-u)$, while t_{pp} in the other direction remains the same compared to the normal lattice (HTT). In figure 8 we compare the energy as a function of u for the diagonal and vertical stripes on a 16×15 lattice. The doping ratio is given by 0.033 corresponding to the lightly doped region. The diagonal striped state has lower energy than the vertical state after level crossing due to the increase of transfer deformation. This supports our scenario concerning the stability of diagonal stripes. With respect to SC, our preliminary calculations indicate the impossibility of coexistence of SC and diagonal stripes. In table 2 we summarize the possible spin structure versus hole-doping rate.

5. Summary

In this paper we have investigated the superconducting and inhomogeneous ground state under the lattice distortions based on the three-band model of high-T_c cuprates using the variational Monte Carlo method. We have studied the correlated states with superconducting and striped antiferromagnetic orders. The inclusion of striped order improves the wavefunction

Table 2. Possible spin structures versus hole-doping rate. The coexisting SC state is also shown, where IC indicates the spatially varied SC order parameter and U means uniform pure d-wave SC. '(Vertical)' indicates that the energies of striped and AF states are almost degenerate.

Lattice	Lightly	Under	Optimally	Overdoped
LTT	Vertical d-wave (IC)	Vertical d-wave (IC)	(Vertical) d-wave	Commensurate d-wave (U)
LTO	Diagonal non SC	Vertical d-wave (IC)	(Vertical) d-wave	Commensurate d-wave (U)

considerably. The decreasing tendency of the SC condensation energy, reported from the specific-heat measurements, is suggested as a result of the reduction of the SC domain in the hole-rich region. The vertical or horizontal stripes are stabilized under the LTT distortion as a cooperative phenomenon of electrons and lattice. An oscillation of the tilt angle is also considered to get the energy gain of doped holes along the stripes. The softening of tilt angles occurs in the hole-rich region, from which we have pointed out a possibility that the stable striped state has hole-rich arrays perpendicular to the tilting axis of the lattice distortions in the LTT phase as shown in figure 7 that can be regarded as the LTT–HTT mixed phase.

Acknowledgments

The author thanks K Yamaji, M Miyazaki, S Koikegami and H Oyanagi for stimulating discussions.

References

[1] Anderson P W 1998 *Science* **279** 1196
[2] Arai M *et al* 1999 *Phys. Rev. Lett.* **83** 608
[3] Bianconi A *et al* 1996 *Phys. Rev. Lett.* **76** 3412
[4] Bickers N E, Scalapino D J and White S R 1989 *Phys. Rev. Lett.* **62** 961
[5] Blankenbecler R, Scalapino D J and Sugar R L 1981 *Phys. Rev.* D **24** 2278
[6] Ceperley D, Chester G V and Kalos K H 1977 *Phys. Rev.* B **16** 3081
[7] Eskes H, Sawatzky G A and Feiner L F 1989 *Physica* C **160** 424
[8] Fleck M, Lichtenstein A I, Pavarini E and Oleś A M 2000 *Phys. Rev. Lett.* **84** 4962
[9] Fleck M, Lichtenstein A I and Oleś A M 2001 *Phys. Rev.* B **64** 134528
[10] Fujita M *et al* 2002 *Phys. Rev. Lett.* **88** 167008
[11] Fujita M *et al* 2002 *Phys. Rev.* B **65** 064505
[12] Giamarchi T *et al* 1990 *Phys. Rev.* B **42** 10641
[13] Harrison W A 1980 *Electronic Structure and Properties of Solids* (San Francisco; CA: Freeman)
[14] Himeda A, Kato K and Ogata M 2002 *Phys. Rev. Lett.* **88** 117001
[15] Hybertson M S, Stechel E B, Schlüter M and Jennison D R 1990 *Phys. Rev.* B **41** 11068
[16] Ichioka M and Machida K 1999 *J. Phys. Soc. Japan* **68** 2168
[17] Ichikawa N *et al* 2000 *Phys. Rev. Lett.* **85** 1738
[18] Kampf A P, Scalapino D J and White S R 2001 *Phys. Rev.* B **64** 052509
[19] Kimura H *et al* 1999 *Phys. Rev.* B **59** 6517
[20] Koike S, Yamaji K and Yanagisawa T 1999 *J. Phys. Soc. Japan* **68** 1657
[21] Koike S, Yamaji K and Yanagisawa T 2000 *J. Phys. Soc. Japan* **69** 2199
[22] Koikegami S and Yanagisawa T 2001 *J. Phys. Soc. Japan* **70** 3499
Koikegami S and Yanagisawa T 2002 *J. Phys. Soc. Japan* **71** 671
[23] Kondo J 2001 *J. Phys. Soc. Japan* **70** 2001
[24] Lee Y S *et al* 1999 *Phys. Rev.* B **60** 3643
[25] Loram J W, Mirza K A, Cooper J R and Liang W Y 1993 *Phys. Rev. Lett.* **71** 1740

[26] Loram J W, Mirza K A, Cooper J R, Athanassopoulou N and Liang W Y 1996 *Proc. 10th Ann. HTS Workshop* (Singapore: World Scientific) p 341
[27] Lorenzano J and Seibold G 2002 *Phys. Rev. Lett.* **89** 136401
[28] Machida K 1989 *Physica* C **158** 192
[29] Matsuda M *et al* 2000 *Phys. Rev.* B **62** 9148
[30] Matveenko S I *et al* 2000 *Phys. Rev. Lett.* **84** 6066
[31] McMahan A K, Annett J F and Martin R M 1990 *Phys. Rev.* B **42** 6268
[32] Migliori A *et al* 1990 *Phys. Rev.* B **41** 2098
[33] Miyazaki M, Yamaji K and Yanagisawa T 2002 *J. Phys. Chem. Solids* **63** 1403
[34] Monthoux P and Scalapino D J 1994 *Phys. Rev. Lett.* **72** 1874
[35] Momono M, Matsuzaki T, Oda M and Ido M 2002 *J. Phys. Soc. Japan* **71** 2832
[36] Mook H A, Pengcheng D, Dogan F and Hunt R D 2000 *Nature* **404** 729
[37] Nakanishi T, Yamaji K and Yanagisawa T 1997 *J. Phys. Soc. Japan* **66** 294
[38] Noack R M *et al* 1997 *Phys. Rev.* B **56** 7162
[39] Pao C-H and Bickers N E 1994 *Phys. Rev.* B **49** 1586
[40] Pao C-H and Bickers N E 1994 *Phys. Rev. Lett.* **72** 1870
[41] Poilblanc D and Rice T M 1989 *Phys. Rev.* B **39** 9749
[42] Schulz H J 1990 *Phys. Rev. Lett.* **64** 1445
[43] Tjeng L H, Eskes H and Sawatzky G A 1989 *Strong Correlation and Superconductivity* ed H Fukuyama, S Maekawa and A P Malozemoff (Berlin: Springer) p 33
[44] Tranquada J M, Sternlieb B J, Axe J D, Nakamura Y and Uchida S 1995 *Nature* **375** 561
[45] Suzuki T *et al* 1998 *Phys. Rev.* B **57** 3229
[46] Wakimoto S *et al* 2000 *Phys. Rev.* B **61** 3699
[47] Yamada K *et al* 1998 *Phys. Rev.* B **57** 6165
[48] Yamaji K, Shimoi Y and Yanagisawa T 1994 *Physica* C **235** 2221
[49] Yamaji K, Yanagisawa T and Koike S 1998 *Physica* C **304** 225
[50] Yamaji K, Yanagisawa T and Koike S 2000 *Physica* B **284–288** 415
[51] Yanagisawa T, Koike S and Yamaji K 1998 *J. Phys. Soc. Japan* **67** 3867
[52] Yanagisawa T, Koike S and Yamaji K 1999 *J. Phys. Soc. Japan* **68** 3867
[53] Yanagisawa T, Koike S and Yamaji K 2000 *Physica* B **284** 467
[54] Yanagisawa T, Koike S and Yamaji K 2001 *Phys. Rev.* B **64** 184509
[55] Yanagisawa T, Koike S, Miyazaki M and Yamaji K 2002 *J. Phys. Condens. Matter* **14** 21
[56] Yanagisawa T, Miyazaki M and Yamaji K 2002 *J. Phys. Chem. Solids* **63** 1379
[57] Yanagisawa T *et al* 2003 Private communication
[58] Yokoyama H and Shiba H 1988 *J. Phys. Soc. Japan* **57** 2482
[59] Zaanen J and Oleś A M 1988 *Phys. Rev.* B **37** 9423
[60] Zaanen J and Gunnarsson O 1989 *Phys. Rev.* B **40** 7391